Microgrid Operation Improvement by Adaptive Virtual Impedance

Mohsen Eskandari [1*], Li Li [2]

[1] Faculty of Engineering and Information Technology, University of Technology Sydney, Ultimo 2007, Sydney, Australia
[*]mohsen.eskandari@student.uts.edu.au

Abstract: Microgrid concept (MG) is regarded as the best solution for optimal integration of the renewable energy sources (RESs) into power systems. However, novel control strategies should be developed because of the distinct inherent feature of MG components in comparison to conventional power systems. Although the droop-based control method is adopted in the MG to share power among distributed generation units, its dependency to grid parameters makes its implementation not as convenient as that in conventional power systems. Virtual impedance has been proposed as the complementary part of droop control in MGs. In this paper, adaptive virtual impedance is designed considering its effects on the system performance in the MG including: 1) Decoupling active and reactive power control by making the grid X/R ratio high, 2) Maximum transferable power through the feeder, 3) Stability concern, 4) Precise reactive power sharing in different operating modes as well as smooth transition from connected mode (CM) to islanded mode (IM). To this end, a novel method is proposed to determine the reactive power reference of distributed generation (DG) units according to their contribution in reactive power sharing in IM. In addition, simulation in MATLAB/SIMULINK environment is conducted to assess the performance of the control system.

1. Introduction

Modern life requirements in terms of providing clean and economically efficient electrical energy have encouraged power engineers to integrate renewable energy sources (RESs) into distribution networks and close to load centres. Over the last two decades, microgrid (MG) concept has provided the idea of optimal and reliable integration of power electronic-based RESs and micro-sources (MSs) as distributed generation (DG) units into power systems. In addition to energy management and power quality improvement, the islanded operation of MG provides reliability enhancement by uninterrupted load supply whenever the upstream network is unavailable [1]-[3].

Output voltage and output power of RESs are controlled by controlling power electronic converters in order to achieve the following goals in different operating modes of MGs: 1) controlling output power of converters in connected mode (CM) according to the set points determined by the MG central controller (MGCC); 2) maintaining the stability of MG by load tracking (holding the balance between production and consumption) in transition from CM to islanded mode (IM); 3) voltage regulation and accurate power sharing in IM [4]. To achieve the above mentioned goals, generally two major types of control strategies have been introduced for MG control systems, centralized and decentralized control strategies [5]. The centralized control systems are based on high-bandwidth communication links, which collect data from each DG unit to the MGCC and send the set points determined by the MGCC to DG units. It has features such as high power quality, poor reliability, fast transient, expensive and complex communication network, and the plug-&-play capability is not feasible. On the other hand, decentralized control systems rely on the performance of local controllers which are based on local variable measurements. Low power quality, acceptable reliability, slow dynamic transient, easy implementation and plug-&-play capability are features of this method [6].

The idea of cooperative operation of local controllers in coordination with the MGCC by low-bandwidth communication links, which takes advantage of both strategies mentioned above, may help to have better control performance in the MG. So, the hierarchical control structure has been proposed to facilitate conducting this control system in the MG [7]-[9]. At the highest level, MGCC is responsible for the energy management [1], while the lowest level is designed to maintain the dynamic stability of MG by holding the balance between production and consumption which is implemented by accurate power sharing and voltage regulation. Droop control, inspired from the synchronous generator behaviour in conventional power systems, is the most prevalent decentralized method among researchers [10]-[13]. In this method, active power and reactive power are controlled by controlling the frequency and voltage, respectively. In spite of effortless implementation, there are some disadvantages related to droop control methods:

1) compromising between power sharing and power quality: power quality is influenced by the droop control, as power sharing implementation requires voltage and frequency to be deviated from the nominal values. Secondary controller in the next level after droop control is in charge of power quality improvement by correcting voltage and frequency deviations [7]-[8].
2) low stability margin as well as insufficiency of droop controller in harmonic and unbalance load condition: some works attempt to address unbalanced and harmonic load sharing as well as stability issues by proposing an extra control level in the hierarchical control structure of MGs [14]-[17].
3) droop controller performance dependency on the grid parameters which is the case in this work: DG units are connected to the MG's main bus, point of common

This work was supported in part by the National Natural Science Foundation of China (NSFC) under Grant 51777078

coupling (PCC), via interfacing feeders including isolating transformer and interconnecting power line. Impedance mismatch of interfacing feeders makes the reactive power sharing inaccurate because of the voltage drop over different feeders. Besides, in order to decouple active and reactive power control loops, X/R ratio of the interconnecting feeder should be high enough [18]-[19].

Some researchers have made efforts to address the reactive power sharing issues in the MG control. In [20] an estimator based adaptive control is developed to predict bus voltage and use it to modify the voltage reference in the droop controller to restore the voltage deviation. Although using an estimator is a good idea to predict the systems states, the estimator's influences on the system performance and the stability concern should be considered in the parameter design. In [21] the droop control is improved to achieve an accurate reactive power sharing between two identical DG units with different feeders. The method is based on injecting low bandwidth synchronization signal which modifies the reference voltage to reduce the error in reactive power sharing. This, in turn, causes a voltage decline, which although is recovered by the proposed method, the power quality is affected. This strategy is based on communication links, and the accuracy of power sharing among different DG units is not clarified. A modified droop control is proposed in [22] by which the historic information of reactive power is used to yield the reactive power sharing among identical DG units, but the system stability is not discussed. The consensus control method (distributed averaging) is adopted in the secondary controller to attain an accurate reactive power sharing as well as voltage regulation in the MG [23]. However, the stability analysis is necessary and the system performance depends on the performance of communication links. An optimal centralized secondary voltage control method is also presented in this paper for multi-bus droop based MGs [24]. Contribution of each DG unit in voltage regulation and reactive power compensation is optimally determined by the MGCC considering MG efficiency, capacity and grid line limits. However, communication network is necessary to collect and send data between the DG units and MGCC. In addition, the computation time for optimization process and communication delay are not discussed. The method presented in [25] relies on the communication link as the MGCC is responsible for coordinating DG units for accurate reactive power sharing by means of sending corresponding signals.

A popular solution which has been proposed to address inaccurate power sharing issues in MGs is virtual impedance. Virtual impedance, primarily, is embedded into the droop control to make the feeder impedance purely inductive to decouple the active and reactive power control [7], [16], [25]-[27]. Some researchers have proposed to employ the virtual impedance as a means of implementing accurate reactive power in MGs [28]-[29]. In [28] an adaptive virtual impedance approach is proposed to remove the impedance mismatch in the feeders. However, the stability analysis is not concluded and the DG units are considered with the same rating. Besides, the proposed method is based on the reference reactive power which is not available in IM for proportional reactive power sharing. In [29] the virtual impedance is regulated adaptively by the consensus control, which as it is mentioned earlier, requires communication links between adjacent DG units and has difficulty in analysing the overall stability of the system.

In this paper, the virtual impedance is designed to improve MG operation in different operating modes. First the permitted band of virtual impedance is deliberated considering its effects on the MG control such as decoupling active and reactive power control, maximum transferable power through the feeder (DG unit capacity and voltage limit) and stability concern. Then the virtual impedance is adjusted within the obtained permitted range adaptively to achieve the following targets: 1) reference tracking in CM where the issue is to deliver the pre-set reactive power determined by the MGCC, 2) smooth transition between CM and IM, 3) accurate reactive power sharing in IM, where the problem is to implement precise reactive power sharing, according to assigned droop gains, by means of voltage regulation to prevent circulating current among power converters. To this end, first a novel decentralized method is developed to specify the reactive power reference for each DG unit according to their contribution in supplying the reactive power. Then, the virtual impedance is adjusted adaptively, employing a PI controller, so that the reference value is tracked. The developed method is fast to avoid the power converter from overloading condition that may lead to collapse of the MG. Besides, the proposed control method is decentralized and does not rely on communication links. The stability analysis is conducted and robustness of the proposed control system is evaluated in the simulation part.

In the next section, the droop-based control system is explained and virtual impedance is designed. In Section 3, a novel control system to improve the MG operation in different operating modes as well as achieving an accurate reactive power sharing in IM is proposed. The simulation results are presented in Section 4 to verify the effectiveness of the proposed control strategy. Finally, Section V draws the conclusion for the paper.

2. Microgrid control system

DG units are connected to the MG via power converters and power flow control and voltage regulation are implemented by controlling the power converter interfaces. For dispatchable DG units, power converters are controlled as Voltage Source Inverter (VSI), see Fig. 1. For non-dispatchable DG units, like RESs, power converters are controlled as Current Source Inverters (CSI) to deliver produced power from natural resources [4]. Nevertheless, RESs can be converted to dispatchable DG units by installing a battery on the DC link side.

2.1. Droop control loop

To design a control system in the MG for an individual DG units, active and reactive power flowing through the feeder are given as, see Fig.1a:

$$P = \frac{1}{Z_{fd}}(V^2\, cos(\theta) - V_o\, V_B\, cos(\delta + \theta)) \quad (1)$$

$$Q = \frac{1}{Z_{fd}}(V^2\, sin(\theta) - V_o\, V_B\, sin(\delta + \theta)) \quad (2)$$

where V_o and V_B are the converter's output voltage and MG main bus voltage, respectively, δ is the phase angle of converter's output voltage, Z_{fd} and θ are the magnitude and the phase angle of the feeder impedance, P and Q are the active and reactive power passing through the feeder. In the conventional power system, the dominant grid impedance is inductive (X/R ratio is high) and θ is approximately 90 degree, then the power flow would be:

$$P = \frac{1}{X_{fd}}(V_o\, V_B\, sin\,\delta) \quad (3)$$

$$Q = \frac{V_o}{X_{fd}}(V_o - V_B\, cos\,\delta) \quad (4)$$

From (3)-(4) it is derived that the active power flow depends on the phase angle (proportional to $|V|^2/X$) and the reactive power flow depends on the voltage difference between DG bus (V_o) and MG bus (V_B) (proportional to $|V|/X$).

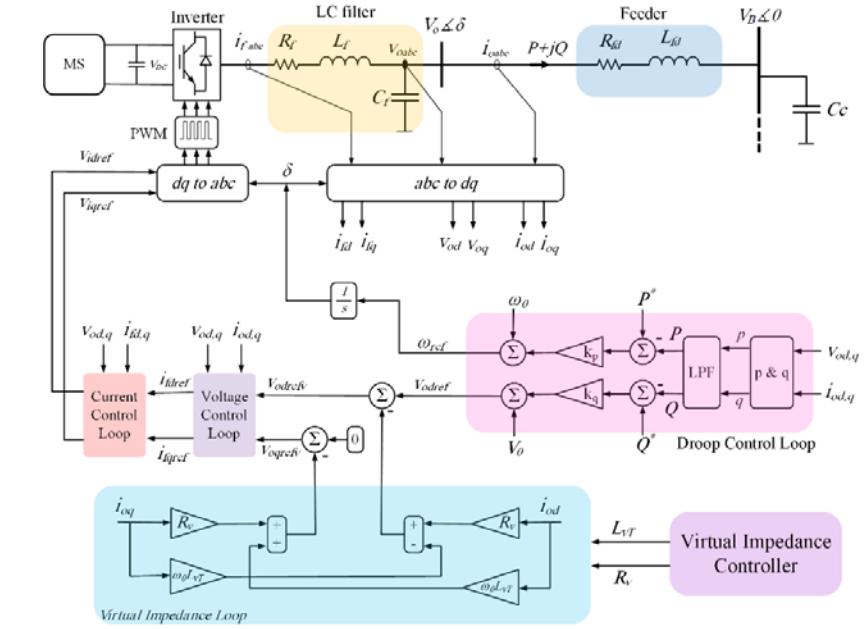

a

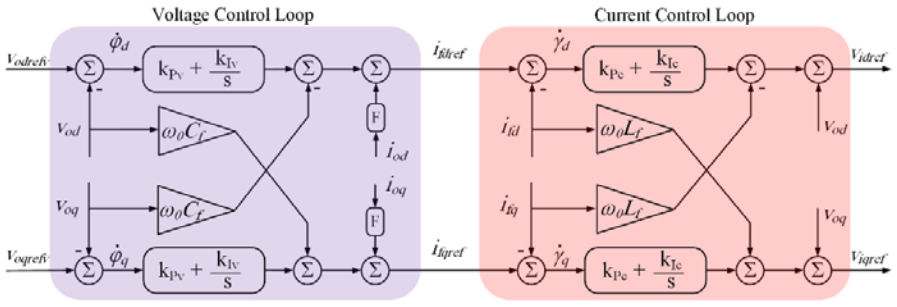

B

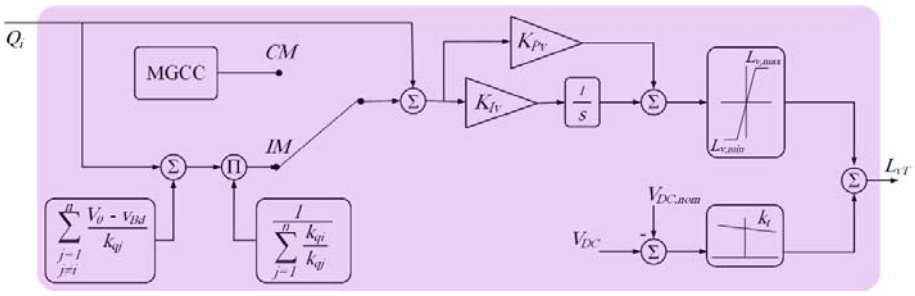

c

Fig. 1. (a) *Control system of a dispatchable DG unit (including MS, DC link and power converter) connected to the MG bus through a feeder. Power converter is a Voltage Source Inverter (VSI) including inverter, LC filter, inner control loops, droop control loop and virtual impedance loop,* ***(b)*** *Cascaded (inner) voltage and current control loops,* ***(c)*** *Block diagram of the proposed adaptive virtual impedance*

So by drooping the frequency (dynamically the phase angle) and voltage magnitude at the converters' output with respect to active power and reactive power variations, the active and reactive power are distributed among DG units proportionally to droop coefficients. Based on droop control, the voltage and frequency are determined as:

$$\omega_{ref} = \omega_0 - k_p(P - P^*) \quad (5)$$

$$\begin{bmatrix} v_{od} \\ v_{oq} \end{bmatrix}_{ref} = \begin{bmatrix} V_0 - k_q(Q - Q^*) \\ 0 \end{bmatrix} \quad (6)$$

where ω_0 and V_0 are the nominal angular frequency and voltage magnitude, respectively, P^* and Q^* the active power and reactive power set points which are determined by the MGCC in CM and are set to zero for dispatchable DG units in the IM. P and Q are average output active and reactive power which are obtained by passing instantaneous active power (p) and reactive power (q) through low pass filter (LPF). ω_{ref} and $v_{o,ref}$ are the converter's output frequency and voltage magnitude determined based on droop control. The control challenge in MGs is that the MG is located in the low voltage grid with low X/R ratio in which the active power and reactive power control is imperfect. Virtual impedance has been proposed to boost X/R ratio and make the conventional *f/P* and *v/Q* droop control possible.

2.2. Virtual impedance design

In order to embed virtual impedance into the control system, the voltage reference is modified as:

$$v_{o,ref,v} = v_{o,ref} - R_v . i_o - L_v \frac{\mathrm{d}i_o}{\mathrm{dt}} \quad (7)$$

where R_v and L_v are the virtual resistance and virtual inductance values, and i_o is the converters output current. By transforming (7) to the direct and quadrature (d-q) reference frame by means of park transformation, in steady state we have:

$$\begin{bmatrix} v_{od} \\ v_{oq} \end{bmatrix}_{ref,v} = \begin{bmatrix} v_{od} \\ v_{oq} \end{bmatrix}_{ref} - R_v \begin{bmatrix} i_{od} \\ i_{oq} \end{bmatrix} - L_v \begin{bmatrix} -\omega_0 i_{oq} \\ +\omega_0 i_{od} \end{bmatrix} = \begin{bmatrix} V_0 - k_q \mathrm{Q} \\ 0 \end{bmatrix} - \begin{bmatrix} R_v & -\omega_0 L_v \\ \omega_0 L_v & R_v \end{bmatrix} \begin{bmatrix} i_{od} \\ i_{oq} \end{bmatrix} \quad (8)$$

The virtual impedance loop is shown in Fig. 1(a). Virtual impedance has been proposed to make the conventional *f-P* and *V-Q* droop control applicable in MGs. However, there are other control aspects which should be considered in designing the virtual impedance and will be discussed in the next subsection.

2.1.1 Decoupling active and reactive power control: According to (3) and (4), the X/R ratio should be high enough to decouple the active and reactive power control. Fig. 2 shows the active and reactive power variations with respect to the increasing phase angle and voltage difference. In Fig. 2(a), it is indicated that, by increasing the phase angle, the delivered active power increases. When X/R ratio is higher than a certain value (X/R>=5), the active power value is saturated and does not increase more with increasing the voltage difference V_o-V_B; see Fig. 2(b). The similar scenario happens for the reactive power in Fig. 2(c-d). Hence, the value of X/R ratio must be greater than a certain value according to (9):

$$\frac{\omega_0(L_{fd} + L_v)}{R_{fd} + R_v} \geq K_1 \quad (9)$$

where R_{fd} and L_{fd} are resistance and inductance of the interconnecting power line (feeder), and K_1 is the minimum permissible value of X/R ratio.

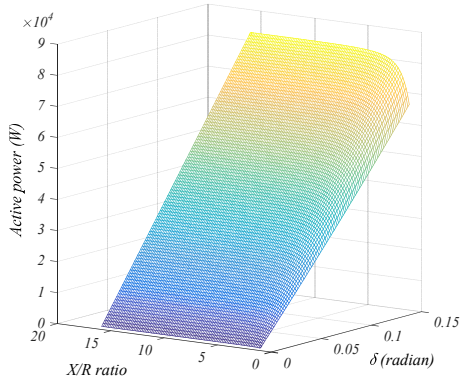

a

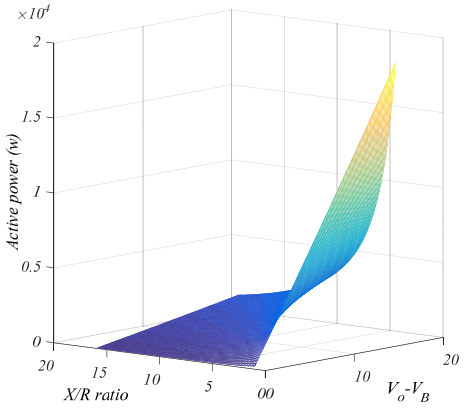

b

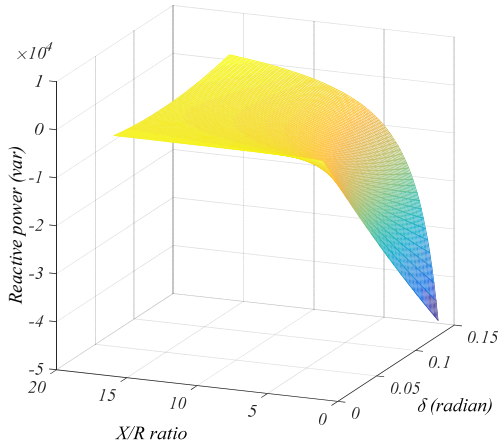

c

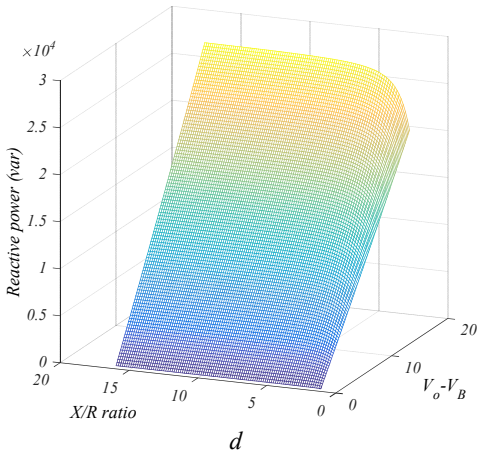

Fig. 2. *Power flow control by voltage and frequency* ***(a)*** *Active power (P)/phase angle (δ)*, **(b)** *Active power (P)/voltage difference (V-V_B)*, **(c)** *Reactive power (P)/phase angle (δ)*, **(d)** *Reactive power (P)/voltage difference (V-V_B)*

2.1.2 Maximum Transferable power: According to (3) and (4), the absolute value of $Z_{fd}=R_{fd}+jX_{fd}$ should not be too high to restrict the transferred power through the feeder. Figs. 3(a-b) show that boosting the X/R ratio by increasing the virtual inductance value restricts the active and reactive power passing through the feeder. The larger virtual inductance, the larger phase angle and voltage difference are required for transferring more active and reactive power, which leads to narrower stability margins and voltage limits concern, respectively. So the absolute value of feeder impedance must be lower than a certain value according to (10):

$$\sqrt{\left(\omega_0 L_{fd}+\omega_0 L_v\right)^2+\left(R_{fd}+R_v\right)^2}\le K_2 \quad (10)$$

where K_2 is the maximum feeder impedance value including physical and virtual elements. Negative virtual resistance may help to increase the transferable power through the feeder. However, stability should be considered in adjusting the virtual inductance and virtual resistance which is discussed in the next subsection.

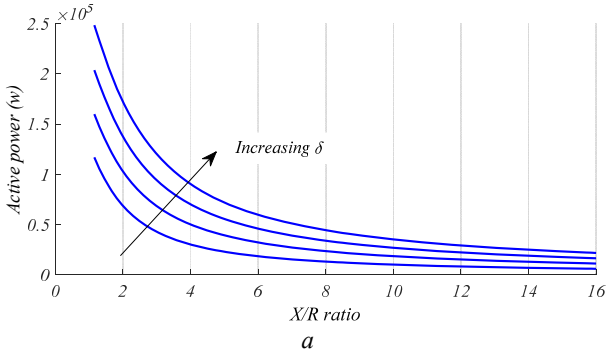

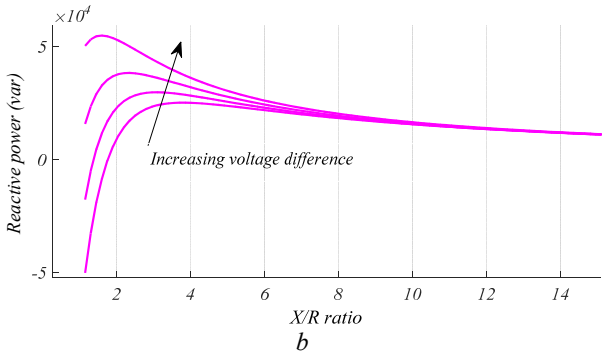

Fig. 3. *Transferable power through the feeder* ***(a)*** *Active power (P),* **(b)** *Rective power (Q)*

2.1.3 Stability concern: In order to develop the state space model of droop-based VSI, first the small signal model of different parts is developed as follows. From *f-P* droop loop, the phase angle dynamics is achieved as:

$$\Delta\dot{\delta}=-k_p.\Delta P \quad (11)$$

The average active and reactive power (P & Q) are achieved after passing instantaneous active and reactive power (p & q) through a first-order filter:

$$\begin{bmatrix}P\\Q\end{bmatrix}=\frac{\omega_c}{s+\omega_c}\left(\begin{bmatrix}v_{od} & v_{oq}\\ v_{oq} & -v_{od}\end{bmatrix}\begin{bmatrix}i_{od}\\ i_{oq}\end{bmatrix}\right) (12)$$

where ω_c is the LPF cutting frequency. After linearization we have:

$$\begin{bmatrix}\Delta\dot{P}\\ \Delta\dot{Q}\end{bmatrix}=\omega_c\left(-\begin{bmatrix}\Delta P\\ \Delta Q\end{bmatrix}+\begin{bmatrix}i_{od0} & i_{oq0}\\ -i_{oq0} & i_{od0}\end{bmatrix}\begin{bmatrix}\Delta v_{od}\\ \Delta v_{oq}\end{bmatrix}+\begin{bmatrix}v_{od0} & v_{oq0}\\ -v_{oq0} & -v_{od0}\end{bmatrix}\begin{bmatrix}\Delta i_{od}\\ \Delta i_{oq}\end{bmatrix}\right) (13)$$

For the VSI's outer (voltage) loop, (see Fig. 1b), we have:

$$\begin{bmatrix}\Delta\dot{\varphi}_d\\ \Delta\dot{\varphi}_q\end{bmatrix}=\begin{bmatrix}-k_q\Delta Q\\ 0\end{bmatrix}-\begin{bmatrix}R_v & -\omega_0 L_v\\ \omega_0 L_v & R_v\end{bmatrix}\begin{bmatrix}\Delta i_{od}\\ \Delta i_{oq}\end{bmatrix}-\begin{bmatrix}\Delta v_{od}\\ \Delta v_{oq}\end{bmatrix} (14)$$

where $\varphi_{d,q}$ are the defined state variables for the voltage controller of VSI. The output of VSI's outer (voltage) control loop is the reference current for the inner (current) control loop. For the current control loop, (see Fig. 1(b)), we have:

$$\begin{bmatrix}\Delta i_{fd,ref}\\ \Delta i_{fq,ref}\end{bmatrix}=F\begin{bmatrix}\Delta i_{od}\\ \Delta i_{oq}\end{bmatrix}+\begin{bmatrix}0 & -\omega_0 C_f\\ \omega_0 C_f & 0\end{bmatrix}\begin{bmatrix}\Delta v_{od}\\ \Delta v_{oq}\end{bmatrix}+\begin{bmatrix}k_{Pv} & 0\\ 0 & k_{Pv}\end{bmatrix}\begin{bmatrix}\Delta\dot{\varphi}_d\\ \Delta\dot{\varphi}_q\end{bmatrix}+\begin{bmatrix}k_{Iv} & 0\\ 0 & k_{Iv}\end{bmatrix}\begin{bmatrix}\Delta\varphi_d\\ \Delta\varphi_q\end{bmatrix} (15)$$

where $i_{fd,ref}$ and $i_{fq,ref}$ are the references for *d-q* components of converter's output LC filter current, C_f is the capacitance of converter's output LC filter, k_{Pv} & k_{Iv} are the proportional and integral gains of voltage PI controller, and F is the feedforward gain of converter's output current to improve the controller performance. For the VSI's inner (current) control loop, we have:

$$\begin{bmatrix}\Delta\dot{\gamma}_d\\ \Delta\dot{\gamma}_q\end{bmatrix}=\begin{bmatrix}\Delta i_{fd,ref}\\ \Delta i_{fq,ref}\end{bmatrix}-\begin{bmatrix}\Delta i_{ld}\\ \Delta i_{lq}\end{bmatrix} \quad (16)$$

where γ_d and γ_q are the defined state variables for the current controller of VSI. The output of current controller is the input voltage reference to the pulse-width modulation module of VSI as:

$$\begin{bmatrix}v_{id,ref}\\ v_{iq,ref}\end{bmatrix}=\begin{bmatrix}v_{od}\\ v_{oq}\end{bmatrix}+\begin{bmatrix}0 & -\omega_0 L_f\\ \omega_0 L_f & 0\end{bmatrix}\begin{bmatrix}i_{fd}\\ i_{fq}\end{bmatrix}+\begin{bmatrix}k_{Pc} & 0\\ 0 & k_{Pc}\end{bmatrix}\begin{bmatrix}\dot{\gamma}_d\\ \dot{\gamma}_q\end{bmatrix}+\begin{bmatrix}k_{Ic} & 0\\ 0 & k_{Ic}\end{bmatrix}\begin{bmatrix}\gamma_d\\ \gamma_q\end{bmatrix} \quad (17)$$

where L_f is the inductance of converter's output LC filter, k_{Pc} and k_{Ic} are the proportional and integral gains of the PI controller in the current control loop. Considering the converter as an ideal switch which transfers the reference voltage to its output, ($v_{id} = v_{id,ref}$ and $v_{iq} = v_{iq,ref}$), the inductance current of LC filter is given as:

$$\begin{bmatrix}\Delta\dot{i}_{fd}\\ \Delta\dot{i}_{fq}\end{bmatrix}=\begin{bmatrix}-R_f/L_f & \omega_{ref}\\ -\omega_{ref} & -r_f/L_f\end{bmatrix}\begin{bmatrix}\Delta i_{fd}\\ \Delta i_{fq}\end{bmatrix}+\frac{1}{L_f}\left(\begin{bmatrix}\Delta v_{id}\\ \Delta v_{iq}\end{bmatrix}-\begin{bmatrix}\Delta v_{od}\\ \Delta v_{oq}\end{bmatrix}\right) \quad (18)$$

where R_f is the resistance of LC filter. For the LC filter capacitance voltage, we have:

$$\begin{bmatrix}\Delta\dot{v}_{od}\\ \Delta\dot{v}_{oq}\end{bmatrix}=\begin{bmatrix}0 & \omega_{ref}\\ -\omega_{ref} & 0\end{bmatrix}\begin{bmatrix}\Delta v_{od}\\ \Delta v_{oq}\end{bmatrix}+\frac{1}{C_f}\left(\begin{bmatrix}\Delta i_{fd}\\ \Delta i_{fq}\end{bmatrix}-\begin{bmatrix}\Delta i_{od}\\ \Delta i_{oq}\end{bmatrix}\right) \quad (19)$$

Finally, for the converter's output current, we have:

$$\begin{bmatrix}\Delta\dot{i}_{od}\\ \Delta\dot{i}_{oq}\end{bmatrix}=\begin{bmatrix}-R_{fd}/L_{fd} & \omega_{ref}\\ -\omega_{ref} & -R_{fd}/L_{fd}\end{bmatrix}\begin{bmatrix}\Delta i_{od}\\ \Delta i_{oq}\end{bmatrix}+\frac{1}{L_{fd}}\left(\begin{bmatrix}\Delta v_{od}\\ \Delta v_{oq}\end{bmatrix}-\begin{bmatrix}\Delta v'_{Bd}\\ \Delta v'_{Bq}\end{bmatrix}\right) \quad (20)$$

where v'_{Bd} and v'_{Bq} are the *d-q* components of MG bus voltage which is transferred to the VSI reference frame (δ) by the transformation matrix as:

$$\begin{bmatrix}v'_{Bd}\\ v'_{Bq}\end{bmatrix}=\begin{bmatrix}\cos\delta & -\sin\delta\\ \sin\delta & \cos\delta\end{bmatrix}\begin{bmatrix}v_{Bd}\\ v_{Bq}\end{bmatrix} \quad (21)$$

Finally, the state space model of VSI is given as:

$$\dot{x}=A.x+B.u \quad (22)$$

where A is the state matrix developed from (11)-(20), B and $u=[v_{Bd}\ v_{Bq}]^T$ are input matrix and input variables to the control system given from (21), and x is the satate variable as:

$$x=\left[\Delta\delta\ \Delta P\ \Delta Q\ \Delta\varphi_d\ \Delta\varphi_q\ \Delta\gamma_d\ \Delta\gamma_q\ \Delta i_{ld}\ \Delta i_{lq}\ \Delta v_{od}\ \Delta v_{oq}\ \Delta i_{od}\ \Delta i_{oq}\right]^T \quad (23)$$

The eigen loci of the VSI including virtual impedance loop is depicted in Fig. 4, which represents the effects of virtual inductance and virtual resistance on the movement of dominant poles of the small signal microgrid model. Increasing the inductance value (arrow direction) moves the critical dominant poles toward the left side of real axis, while the virtual negative resistance has an inverse effect by moving the poles toward the right side of real axis. So the virtual impedance should be adjusted properly. The conventional output feedback methods or a novel optimization algorithm and a suitable objective function, e.g. desired pole locations, may be employed to determine the virtual impedance, which is not discussed in this paper.

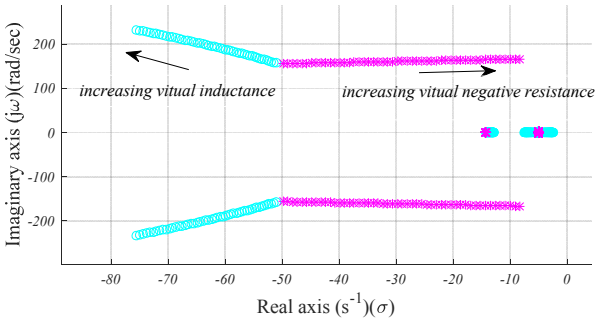

Fig. 4. *Eigenvaue loci*

3. Power sharing and voltage regulation

Power converters are employed at two operating modes in MGs: 1) CSI which follows active and reactive power set points well, but without voltage regulation capability, and is suitable for operating in CM; 2) VSI with voltage regulation capability which is needed for IM operation. The VSI is adopted in both operating modes in this work to have a smooth transition from CM to IM. In order to dispatch power among parallel dispatchable DG units in IM and to avid circulating current among them, VSI is equipped with a droop control loop as the output power control loop. However, the output power of VSI depends on its output voltage and interconnecting power line impedance, which causes inaccurate reactive power sharing because of the voltage drop through the feeders [19]. In this paper, virtual impedance is adjusted adaptively in the permitted band to overcome droop controller disadvantages in power sharing and voltage regulation.

3.1. Connected mode

In CM, DG units deliver the active and reactive power according to the set points determined by the MGCC; see (5) and (6). VSI converters with droop-based control loop deliver the active power as specified by P^*, because frequency is a global variable and sensitivity of the active power to phase angle is high. But, the reactive power is not delivered to be equal to Q^*, as the voltage of MG bus is a local variable. Therefore, the adaptive virtual impedance is adopted to control VSI output reactive power according to (24):

$$L_v=K_{Pv}(Q-Q^*)+K_{Iv}\int(Q-Q^*)dt \quad (24)$$

$$L_{v,min} \le L_v \le L_{v,max}$$

where K_{Pv}, K_{Iv} are the proportional and integral gains of PI controller, respectively, $L_{v,min}$ & $L_{v,max}$ are the minimum and maximum values of virtual inductance which are determined based on the previous section.

3.2. Transition from CM to IM

In CM, DG units follow the active and reactive power set points determined by the MGCC, and the load variation is responded through the main grid. Whenever the main grid is unavailable, dispatchable DG units are responsible for maintaining the balance between the generation and consumption. So if the MG receives considerable power from the main grid in CM, in transition from CM to IM, the output power of dispatchable DG units increases sharply, which results in a voltage drop in the DC link because of the slow response of primary MS. So an energy storage system (ESS) is required in the MG as a spinning reserve to compensate the slow response of micro-sources [30]. Virtual impedance is adjusted to limit the output power of dispatchable units, while the ESS is responsible for the load tracking according to (25):

$$L_{vT} = L_v + L_{vt}$$
$$L_{vt} = -k_t\left(V_{DC} - V_{DC,nom}\right) \quad (25)$$

where L_{vt} is the transient virtual inductance, L_{vT} is the total value of virtual inductance, V_{DC}, $V_{DC,nom}$ are the voltage and nominal voltage of the *DC* link respectively, and k_t is the virtual inductance/DC voltage droop coefficient.

3.3. Islanded mode

In the IM operation, DG units are responsible for supplying the demanded load and for supporting reactive power according to their available capacity and current limits. Therefore, the reference active and reactive power (P^* & Q^*) are zero and power sharing is implemented proportionally to the droop gains so that (26)-(27) are established:

$$k_{q1}Q_1 = k_{q2}Q_2 = \cdots = k_{qn}Q_n \quad (26)$$
$$k_{p1}P_1 = k_{p2}Q_2 = \cdots = k_{pn}P_n \quad (27)$$

However, the output reactive power of VSIs depends on the feeder impedance and voltage difference between the terminal buses. Voltage drop in the feeder causes an inaccurate reactive power sharing among DG units which are connected to the MG bus with different feeder impedances. Therefore, voltage regulation and accurate reactive power sharing appear as a crucial issue which may cause the circulating current among DG units. Besides, this may even lead to the MG collapse as the semiconductor devices suffer from narrow current limits. Nonetheless, if the contribution of individual DG units in supporting the demanded reactive power (Q^*) is estimated according to corresponding droop gains, the adaptive virtual impedance can be adopted to implement reactive power sharing according to (26). To this end, first the reference reactive power of each DG unit is estimated as follows. To estimate the voltage drop in the feeder including that caused by the virtual impedance, according to park transformation for resistive-inductive lines, we have:

$$\begin{bmatrix} v_{od} - v_{Bd} \\ v_{oq} - v_{Bq} \end{bmatrix} = \begin{bmatrix} R_{fdi} + R_{vi} & -\omega_0\left(L_{fdi} + L_{vi}\right) \\ \omega_0\left(L_{fdi} + L_{vi}\right) & R_{fdi} + R_{vi} \end{bmatrix} \begin{bmatrix} i_{od} \\ i_{oq} \end{bmatrix} \quad (28)$$

To calculate the VSI's output active and reactive power by means of the *d-q* component of the VSI's output voltage and current, we have:

$$\begin{bmatrix} P \\ Q \end{bmatrix} = \begin{bmatrix} v_{od} & v_{oq} \\ v_{oq} & -v_{od} \end{bmatrix} \begin{bmatrix} i_{od} \\ i_{oq} \end{bmatrix} \quad (29)$$

where P and Q are the VSI's output active and reactive power, respectively. In the symmetric three-phase systems, V_q is fixed to zero. By substituting the current component from (30) into (29) we have:

$$\begin{bmatrix} v_{od} - v_{Bd} \\ v_{oq} - v_{Bq} \end{bmatrix} = \frac{1}{v_{od}} \begin{bmatrix} R_{fdi} + R_{vi} & \omega_0\left(L_{fdi} + L_{vi}\right) \\ \omega_0\left(L_{fdi} + L_{vi}\right) & -R_{fdi} - R_{vi} \end{bmatrix} \begin{bmatrix} P \\ Q \end{bmatrix} \quad (30)$$

Then the *d-q* component of voltage profile in the feeder for a given DG unit (DG *i*) is obtained as:

$$\begin{bmatrix} v_{Bd} \\ v_{Bq} \end{bmatrix} = \begin{bmatrix} V_0 - k_{qi}Q_i \\ 0 \end{bmatrix} - \frac{1}{v_{od}} \begin{bmatrix} R_{fdi} + R_{vi} & \omega_0\left(L_{fdi} + L_{vi}\right) \\ \omega_0\left(L_{fdi} + L_{vi}\right) & -R_{fdi} - R_{vi} \end{bmatrix} \begin{bmatrix} P_i \\ Q_i \end{bmatrix} \quad (31)$$

The first item at the right hand side of (31) is the DG unit output voltage which is specified by the droop controller. The second term is the voltage drop over the feeder impedance and virtual impedance. In order to compensate the voltage drop over the feeder impedance and virtual impedance, it is proposed to modify the reference voltage of i^{th} DG unit in (8) as the following:

$$\begin{bmatrix} v_{od} \\ v_{oq} \end{bmatrix}_{ref,vi} = \begin{bmatrix} V^* - k_{qi}Q_i \\ 0 \end{bmatrix} - \begin{bmatrix} R_{vi} & -\omega_0 L_{vi} \\ \omega_0 L_{vi} & R_{vi} \end{bmatrix} \begin{bmatrix} i_{odi} \\ i_{oqi} \end{bmatrix} + \frac{1}{v_{od}} \begin{bmatrix} R_{fdi} + R_{vi} & \omega_0\left(L_{fdi} + L_{vi}\right) \\ \omega_0\left(L_{fdi} + L_{vi}\right) & -R_{fdi} - R_{vi} \end{bmatrix} \begin{bmatrix} P_i \\ Q_i \end{bmatrix} \quad (32)$$

The third item at the right hand side of (32) is added to compensate voltage drop through the feeder and voltage drop caused by virtual impedance. It is worth noting that both the virtual impedance loop and voltage drop compensation loop in (32) are effective as they have different time constant because of the low pass filter for P and Q measurements. Then the voltage at MG bus is given as:

$$\begin{bmatrix} v_{Bd} \\ v_{Bq} \end{bmatrix} = \begin{bmatrix} V_0 - k_{qi}Q_i \\ 0 \end{bmatrix} \quad (33)$$

So the output reactive power of i^{th} DG unit is obtained as:

$$Q_i = \frac{V_0 - v_{Bd}}{k_{qi}} \quad (34)$$

And the total reactive power (Q_T) is give as:

$$Q_T = \sum_{i=1}^{n} Q_i = \sum_{i=1}^{n} \frac{V_0 - v_{Bd}}{k_{qi}} \quad (35)$$

In this way, the total reactive power is estimated at each DG unit using only local measurements. Finally, the reference reactive power of DG *i* is determined as:

$$Q_{iIM}^{*} = \frac{1}{\sum_{j=1}^{n} \frac{k_{qi}}{k_{qj}}} Q_T \quad (36)$$

where Q^*_{iIM} is the reference reactive power of i^{th} DG unit in the islanded mode operation which is achieved according to the droop gains. The PI controller presented in (24) is adopted to tune the virtual impedance adaptively to implement the accurate reactive power sharing. The proposed adaptive virtual impedance loop is represented in Fig. 1(c).

3.3.1 Stability analysis: In order to incorporate the adaptive virtual inductance and the proposed method into the state space model of VSI which is presented earlier, a new state variable is defined as:

$$\dot{\beta} = Q - Q^{*} \quad (37)$$

And the dynamics of adaptive virtual inductance is determined according to (24) as:

$$\Delta L_v = K_{Pvi}\ (\Delta Q - \Delta Q^{*}) + K_{Ivi}\,.\Delta\beta \quad (38)$$

where ΔQ^* is obtained from (35)-(36) as:

$$\Delta Q^{*} = {-\Delta v_{Bd}}/{k_q} \quad (39)$$

Now the problem is to determine dynamic of voltage at the MG bus (v_{Bd}). Since the voltage dynamics at PCC is determined by droop controllers in IM, it cannot be considered as input to the control system. So the voltage dynamics at the MG bus is modelled by the shunt compensator capacitor, load current and current from DG units as:

$$\begin{bmatrix} \Delta\dot{v}_{Bd} \\ \Delta\dot{v}_{Bq} \end{bmatrix} = \begin{bmatrix} 0 & \omega_0 \\ -\omega_0 & 0 \end{bmatrix} \begin{bmatrix} \Delta v_{Bd} \\ \Delta v_{Bq} \end{bmatrix} + \frac{1}{C_c} \left(\begin{bmatrix} \Delta i_{od} \\ \Delta i_{oq} \end{bmatrix} - \begin{bmatrix} \Delta i_{Ld} \\ \Delta i_{Lq} \end{bmatrix} \right) \quad (40)$$

where C_c is the capacitance of shunt compensator and i_L is the load current considered as the disturbance. The state variable related to voltage control loop, given in (14) are modified according to (32) and (38) as:

$$\begin{bmatrix} \Delta\dot{\varphi}_d \\ \Delta\dot{\varphi}_q \end{bmatrix} = -\begin{bmatrix} R_v & -\omega_0 L_{v0} \\ \omega_0 L_{v0} & R_v \end{bmatrix} \begin{bmatrix} \Delta i_{od} \\ \Delta i_{oq} \end{bmatrix} - \omega_0 \begin{bmatrix} 0 & -\Delta L_v \\ \Delta L_v & 0 \end{bmatrix} \begin{bmatrix} i_{od0} \\ i_{oq0} \end{bmatrix} + \left(\begin{bmatrix} 0 & -k_q \\ 0 & 0 \end{bmatrix} + \frac{1}{V_0} \begin{bmatrix} R_{fd} + R_v & \omega_0 (L_{fd} + L_{v0}) \\ \omega_0 (L_{fd} + L_{v0}) & -R_{fd} - R_v \end{bmatrix} \right) \begin{bmatrix} \Delta P \\ \Delta Q \end{bmatrix} + \frac{\omega_0}{V_0} \begin{bmatrix} 0 & \Delta L_v \\ \Delta L_v & 0 \end{bmatrix} \begin{bmatrix} P_0 \\ Q_0 \end{bmatrix} - \begin{bmatrix} \Delta v_{od} \\ \Delta v_{oq} \end{bmatrix} \quad (41)$$

where L_{v0}, i_{od0}, i_{oq0}, P_0 and Q_0 are the corresponding values at the operation condition. The Eigen loci of the proposed method is compared with conventional droop controller, see Fig. 5. Two *f-P* and *V-Q* are strongly coupled in the conventional droop controller because of low X/R ratio of the feeder. Increasing the droop gain of a given loop moves the eigenvalues of the other loop, Fig. 5a. On the other hand, the proposed method not only decouples the two droop loops, it also improves the stability margins compared to the conventional droop controller, Fig. 5b.

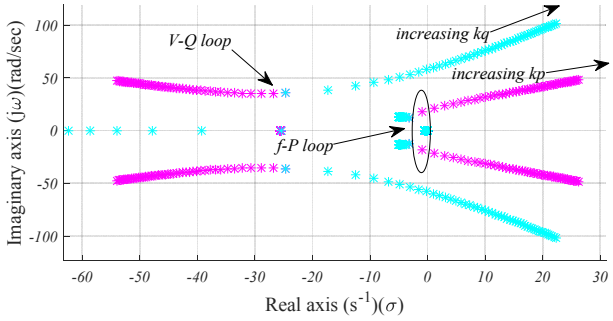

a

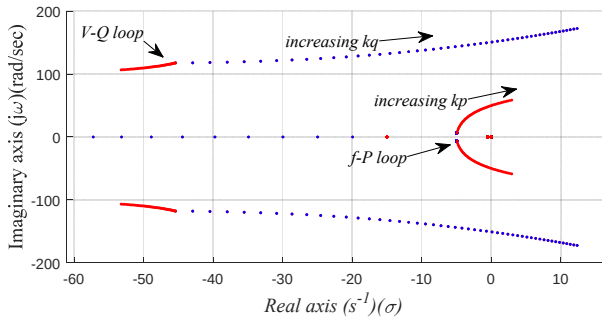

b

Fig. 5. *Eigen loci*
(a) *Conventional droop control (P),* **(b)** *Proposed method*

4. Simulation results

A MG with three DG units is simulated in the MATLAB/SIMULINK to assess the performance of the proposed control strategy, as shown in Fig. 6. The MG is connected to main grid at PCC through a distribution transformer. The main grid is simulated with a synchronous generator block which is available in the Simscape/Power Systems toolbox. The parameters of MG and DG units are presented in Table 1.

Case 1 (S_3, S_{13} & S_{23} are open). In this case, DG 1 and DG 2 are considered as the dispatchable units and

responsible for load sharing. The contribution of both DG units is considered equal in this case. Consequently, the two DGs have the same *V-Q* droop gain of 0.00025. The simulation results are shown in Fig. 7. The MG is isolated at t=0.15 sec when the exchanged power between the MG and main grid becomes zero. Using the conventional droop control, in CM, VSIs do not follow the reactive reference (Q^*=4000); in IM, although the droop coefficients are same, the reactive power is not shared equally between the two DG units because of the feeder impedance mismatch and voltage drop in the feeder; see Fig. 7(a). Employing the proposed control strategy to adjust the virtual impedance adaptively, the desired reactive power sharing is achieved; see Fig. 7(c). The active power sharing is also improved using the adaptive virtual impedance; see Fig. 7(d).

TABLE 1 SYSTEM PARAMETERS

	Parameters	Values
Grid	AC voltage (V_{RMS})/phase	230
	Frequency (Hz)	60
	DC link voltage (V)	850
Filter	L inductance (H)	1.35e-3
	C capacitance (μF)	50
	L resistance (Ω)	0.1
DG #1	Power rating	40 kW, 20kVar
	Feeder inductance (H)	5.1e-4
	Feeder resistance (Ω)	0.04
	V-Q coefficient	0.00025
	f-P coefficient	0.00001
DG #2	Power rating	30 kW, 15kVar
	Feeder inductance (H)	6.63e-4
	Feeder resistance (Ω)	0.052
	V-Q coefficient	0.0005
	f-P coefficient	0.00002
DG #3	Power rating	20 kW, 10kVar
	Feeder inductance (H)	3.06e-4
	Feeder resistance (Ω)	0.024
	V-Q coefficient	0.0005
	f-P coefficient	0.00002

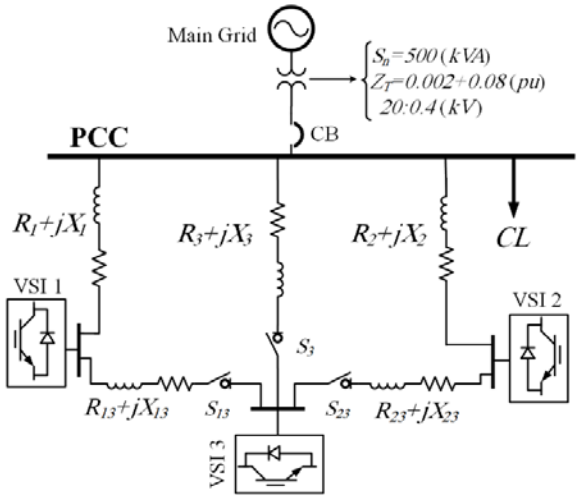

Fig. 6. *Schematic diagram of the simulated MG. CL: Common Load; CB: Circuit Breaker; S: Switch*

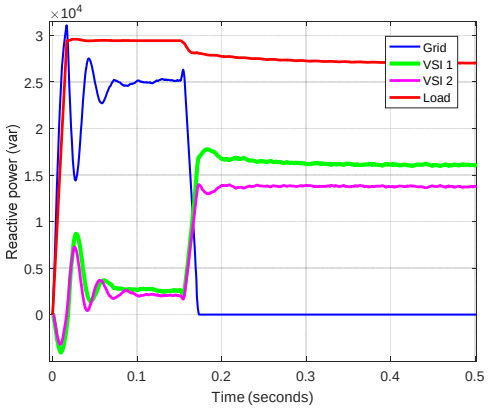

a

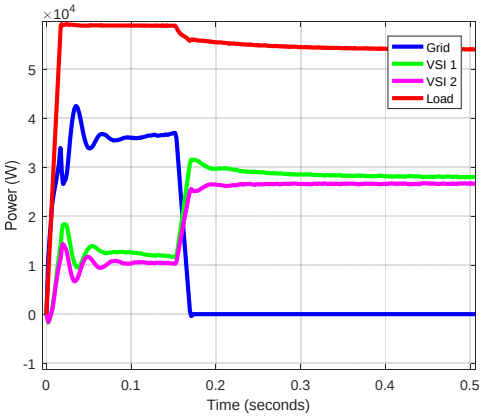

b

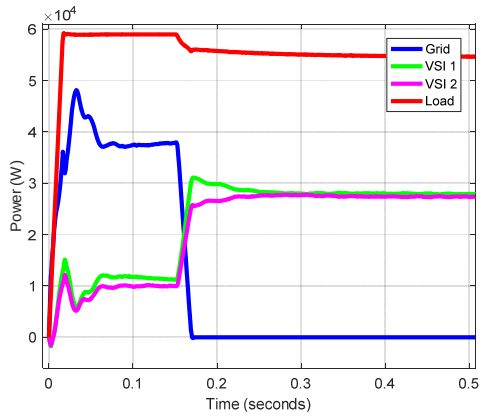

c

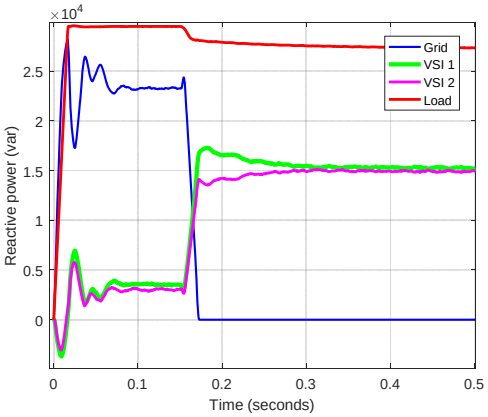

d

Fig. 7. *Power sharing in MG (MG is disconnected at t=0.15),* ***(a), (b)*** *Conventional droop control,* ***(c), (d)*** *Proposed adaptive virtual impedance*

Case 2 (S_3, S_{13} & S_{23} are open). In this case, DG 1 and DG 2 are considered in the simulation, and the contribution of DG 1 is twice as DG 2 according to the data given in Table I. Fig. 8 shows the results in which the transition from CM to IM is indicated by the zero reactive power received from the grid. In CM, DG units deliver reactive power as the reactive reference is set by MGCC; and in IM, the reactive power is dispatched between the two DG units according to the droop coefficients which are set by MGCC. The adaptive virtual impedances are indicated in Fig. 8(c).

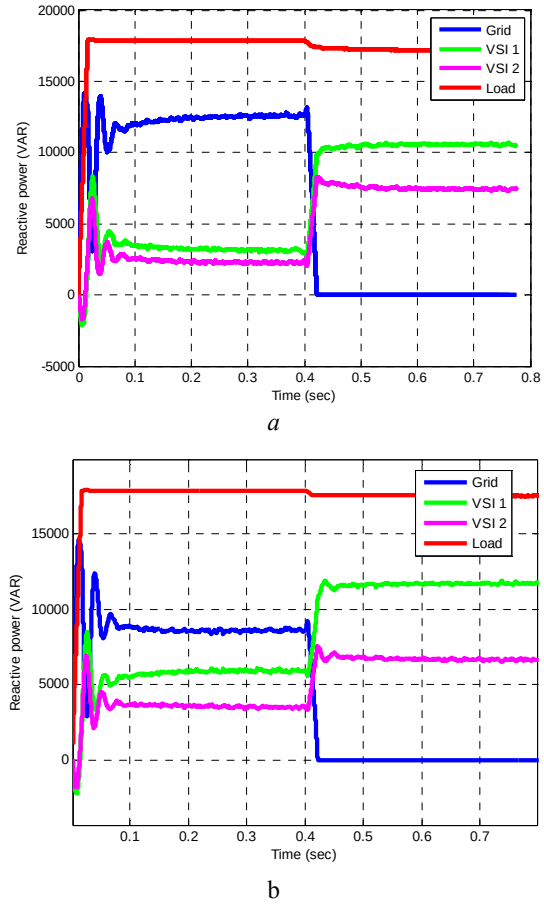

Fig. 8. *Reactive power sharing in MG between DG 1 and DG 2,* ***(a)*** *Conventional droop control,* ***(b)*** *Proposed adaptive virtual impedance*

Case 3 (CB, S_3, S_{13} & S_{23} are open). In this case, the scenario is similar to the case 2 except that the whole simulation is run in IM. The simulation results are depicted in the Fig. 9. The adaptive virtual impedances are shown in Fig. 9(c).

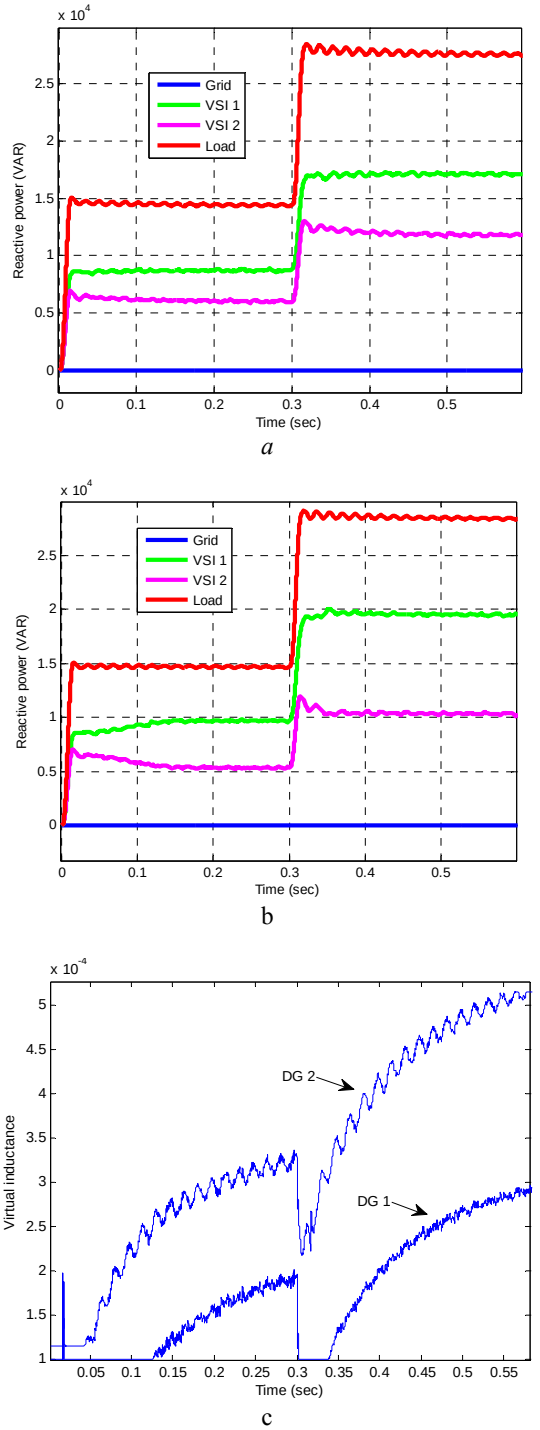

Fig. 9. *Reactive power sharing in isolated MG,* ***(a)*** *Conventional droop control,* ***(b)*** *Proposed adaptive virtual impedance,* ***(c)*** *Adaptive virtual inductance values*

Case 4 (S_3 is closed, S_{13} & S_{23} are open). In this case, all three DG units are considered in the simulation and the contribution of all DGs are given equally by assigning the same *V-Q* droop gain of 0.00025. The simulation results are shown in Fig. 10.

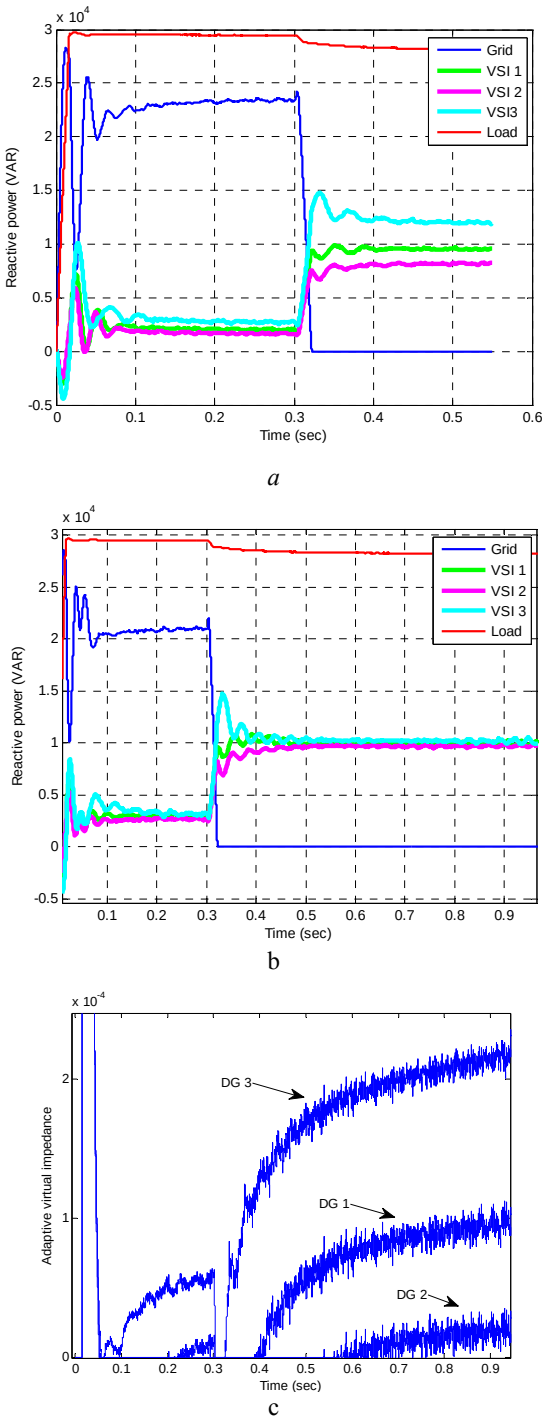

Fig. 10. *Reactive power sharing in MG among DG 1, DG 2 and DG 3,* ***(a)*** *Conventional droop control,* ***(b)*** *Proposed adaptive virtual impedance,* ***(c)*** *Adaptive virtual inductance values*

Case 5 (S_3 is closed, CB, S_{13} & S_{23} are open). In this case, all the three DG units are considered in the simulation and the contribution of DG units are determined according to the data in Table 1. The simulation results are shown in Fig. 11. In order to demonstrate validity and superiority of the proposed method, the simulation results in this case are also compared with the consensus control-based technique which recently has become popular among researchers [18], [23]. The control performance of consensus control is depicted in Fig. 11(c). Comparing Fig. 11(b) and Fig. 11(c) reveals that, in addition to accuracy, the quick response is another advantage of the proposed control method over the consensus control as the time constant of the proposed method is 0.2 second while it is 2 seconds for the consensus control. Since, in contrast to conventional synchronous generators, power converters have a limited Amp×time tolerable band, the reactive power sharing must be implemented immediately to prevent the corresponding protection relays from operation. Otherwise, it may lead to cascading outage of DG units and eventually instability of the MG.

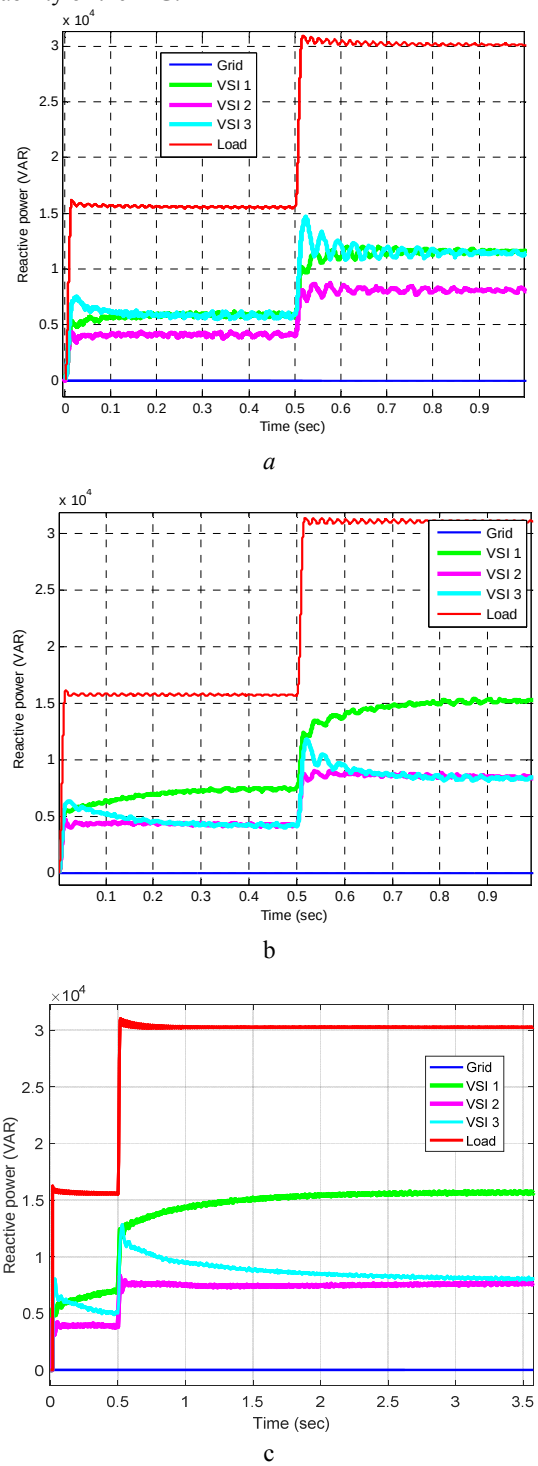

Fig. 11. *Reactive power sharing in MG among DG 1, DG 2 and DG 3,* ***(a)*** *Conventional droop control,* ***(b)*** *Proposed adaptive virtual impedance,* ***(c)*** *Consensus control,*

Case 6 (S_{13} & S_{23} are closed, CB & S_3 are open). In order to analyse robustness of the control system with respect to parameters and network topology uncertainties, three identical DG units are connected to a meshed MG. X/R ratio of the power lines is also reduced from 4 in cases 1-5 to 2 in this case. The simulation results are presented in Fig. 12. Although the system becomes more oscillatory because of the meshed topology and low X/R ratio, the control system is still able to stabilise the MG. Besides, reactive power sharing is implemented accurately. The only requirement of the proposed method is that the direct component of voltage at PCC should be sent to the DG units which are not connected to the PCC directly, as PCC voltage cannot be estimated in decentralized form in those DGs. This is not a big challenge, however, as the existing low band-width communication link is sufficient to send a DC value.

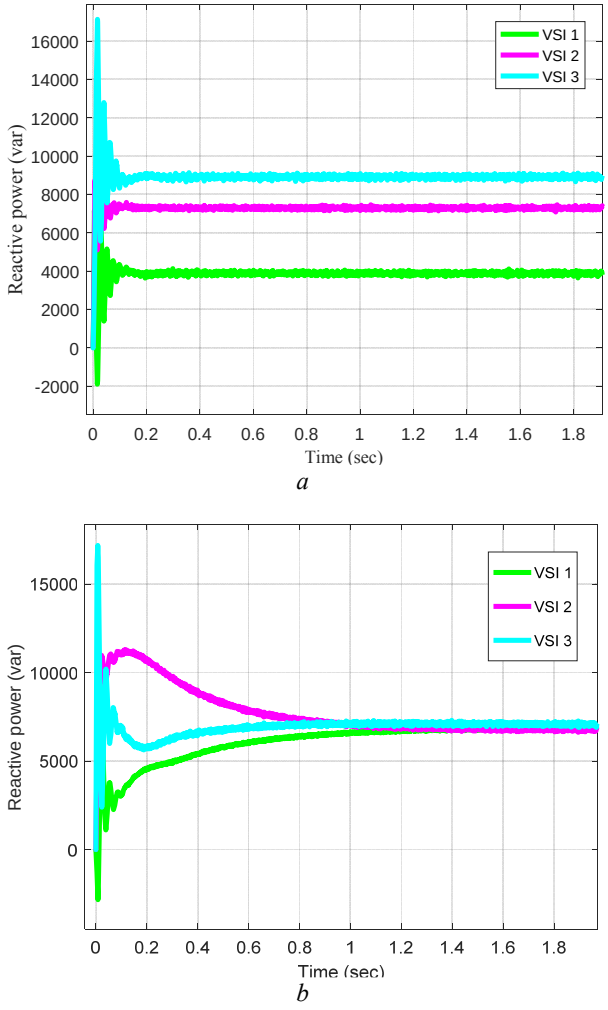

Fig. 12. *Reactive power sharing in the MG among DG 1, DG 2 and DG 3,* ***(a)*** *Conventional droop control,* ***(b)*** *Proposed adaptive virtual impedance,*

5. Discussion

This paper addresses active and reactive power sharing issues in decentralized droop controlled MGs. However, there are some more problems related to droop control in MGs which should be addressed. The reduction in the active and reactive power of load, when the MG switches from CM to IM, is due to voltage drop caused by droop controllers. Since the constant impedance (at nominal voltage) load block is used in the simulation, voltage drop causes reduction in load. This is a power quality issue related to the droop controller which is not tackled in this work. Moreover, the active and reactive power oscillations in CM comes from the interaction of main grid and voltage sources in the MG. In practical situations, the main grid is always on, and MG is connected after synchronization process. The synchronization scheme is beyond the scope of this paper and is not considered in the simulation. On the other hand, the oscillations are mitigated in the isolated MGs (c.f. cases 3 and 5), due to the virtual impedance and modified droop control (32). The virtual impedance and P & Q feedback loops in (32) act like state feedback loops which improve dynamic performance of the controlled system.

6. Conclusion

In this work, virtual impedance is considered as a complementary part of droop-based control system in MGs. First, virtual impedance is modelled into the small signal model of MG. It is shown that virtual impedance should be appropriately designed to decouple the active and reactive power control, and also be bounded for not limiting the maximum transferable power. Negative virtual resistance is proposed to help determine the virtual impedance so that the desired performance is achieved. The root locus of the dominant poles of small signal MG model is drawn to show the effectiveness of the idea. Then, a control strategy is developed to adjust the virtual impedance adaptively so that the smooth transition from the connected mode to islanded mode as well as the accurate reactive power sharing is accomplished. In addition, a novel decentralized method to obtain the reactive power reference based on the contribution of each dispatchable DG unit in reactive power sharing is proposed. Voltage quality is also improved by proposing a method to modify the voltage reference of VSIs. The performance of the proposed control system is evaluated by simulating a typical MG in MATLAB/SIMULINK.

7. References

[1] Moradi, M.H., Eskandari, M. and Hosseinian, S.M.: 'Operational strategy optimization in an optimal sized smart microgrid. IEEE Transactions on Smart Grid, 2015, 6, (3), pp 1087-1095.

[2] Moradi, M.H., Eskandari, M. and Hosseinian, S.M.: 'Cooperative control strategy of energy storage systems and micro sources for stabilizing microgrids in different operation modes. International Journal of Electrical Power & Energy Systems, 2016. 78, pp.390-400.

[3] Moradi, M.H., Eskandari, M. and Showkati, H.: 'A hybrid method for simultaneous optimization of DG capacity and operational strategy in microgrids utilizing renewable energy resources. International Journal of

Electrical Power & Energy Systems, 2014, 56, pp.241-258.
[4] Rocabert, J., Luna, A., Blaabjerg, F. and Rodriguez, P.: 'Control of power converters in AC microgrids. IEEE transactions on power electronics, 2012, 27, (11), pp.4734-4749.
[5] Olivares, D.E., Mehrizi-Sani, Amir H. Etemadi, et al.: 'Trends in microgrid control. IEEE Transactions on smart grid, 2014, 5 (4), pp.1905-1919.
[6] Divshali, P.H., Alimardani, A., Hosseinian, S.H. and Abedi, M.: 'Decentralized cooperative control strategy of microsources for stabilizing autonomous VSC-based microgrids. IEEE transactions on power systems, 2012, 27 (4), pp.1949-1959.
[7] Guerrero, J. M., Vasquez J. C., José Matas, Luis García De Vicuña, and Castilla, M.: 'Hierarchical control of droop-controlled AC and DC microgrids—A general approach toward standardization. IEEE Transactions on industrial electronics, 58, no. 1 (2011): 158-172.
[8] Guerrero, J. M., Chandorkar, M. Tzung-Lin Lee, and Poh Chiang Loh.: 'Advanced control architectures for intelligent microgrids—Part I: Decentralized and hierarchical control. IEEE Transactions on Industrial Electronics, 60, no. 4 (2013): 1254-1262.
[9] Baghaee, H. R., Mirsalim, M and Gharehpetian, G. B.: 'Performance improvement of multi-DER microgrid for small-and large-signal disturbances and nonlinear loads: novel complementary control loop and fuzzy controller in a hierarchical droop-based control scheme. IEEE Systems Journal, 12, no. 1(2016): 444-451.
[10] Planas, E., Gil-de-Muro, A., Andreu, J., Kortabarria, I. and de Alegría, I.M.: 'Design and implementation of a droop control in d–q frame for islanded microgrids. IET Renewable Power Generation, 2013, 7, (5), pp.458-474.
[11] Majumder, R., Ghosh, A., Ledwich, G. and Zare, F.: 'Load sharing and power quality enhanced operation of a distributed microgrid. IET Renewable Power Generation, 2009, 3, (2), pp.109-119.
[12] de Souza, W.F., Severo-Mendes, M.A. and Lopes, L.A.: 'Power sharing control strategies for a three-phase microgrid in different operating condition with droop control and damping factor investigation. IET Renewable Power Generation, 2015, 9, (7), pp.831-839.
[13] Ramezani, M., Li, S. and Sun, Y.: 'Combining droop and direct current vector control for control of parallel inverters in microgrid. IET Renewable Power Generation, 2016, 11, (1), pp.107-114.
[14] Baghaee, H. R. Mirsalim, M. Gevork B. Gharehpetan, and Talebi, H. A.: 'Nonlinear load sharing and voltage compensation of microgrids based on harmonic power-flow calculations using radial basis function neural networks. IEEE Systems Journal, 12, no. 3 (2018), 2749-2759.
[15] Baghaee, H. R. Mirsalim, and M. Gevork B.: 'Real-time verification of new controller to improve small/large-signal stability and fault ride-through capability of multi-DER microgrids. IET Generation, Transmission & Distribution 10, no. 12 (2016): 3068-3084.
[16] Baghaee, H. R. Mirsalim, and M. Gevork B.: 'Power calculation using RBF neural networks to improve power sharing of hierarchical control scheme in multi-DER microgrids. IEEE Journal of Emerging and Selected Topics in Power Electronics 4, no. 4 (2016): 1217-1225.
[17] Baghaee, H. R. Mirsalim, M. Gevork B. Gharehpetan, and Talebi, H. A.: 'Unbalanced harmonic power sharing and voltage compensation of microgrids using radial basis function neural network-based harmonic power-flow calculations for distributed and decentralised control structures. IET Generation, Transmission & Distribution 12, no. 7 (2018): 1518-1530.
[18] Li, Y.W. and Kao, C.N.: 'An accurate power control strategy for power-electronics-interfaced distributed generation units operating in a low-voltage multibus microgrid. IEEE Transactions on Power Electronics, 2009, 24, (12), pp.2977-2988.
[19] M. Eskandari, L. Li, and M. H. Moradi, "Decentralized Optimal Servo Control System for Implementing Instantaneous Reactive Power Sharing in Microgrids," IEEE Transactions on Sustainable Energy, vol. 9, no. 2, pp. 525-537, 2018.
[20] Wang, Y., Chen, Z., Wang, X., Tian, Y., Tan, Y. and Yang, C.: 'An estimator-based distributed voltage-predictive control strategy for AC islanded microgrids. IEEE Transactions on Power Electronics, 2015, 30, (7), pp.3934-3951.
[21] Han, H., Liu, Y., Sun, Y., Su, M. and Guerrero, J.M.: 'An improved droop control strategy for reactive power sharing in islanded microgrid. IEEE Transactions on Power Electronics, 2015, 30 (6), pp.3133-3141.
[22] Sun, X., Hao, Y., Wu, Q., Guo, X. and Wang, B.: 'A multifunctional and wireless droop control for distributed energy storage units in islanded AC microgrid applications. IEEE Transactions on Power Electronics, 2017, 32, (1), pp.736-751.
[23] Simpson-Porco, J. W., Shafiee, Q., Florian Dörfler, et. al.: 'Secondary frequency and voltage control of islanded microgrids via distributed averaging. IEEE Transactions on Industrial Electronics, 2015, 62, (11), pp.7025-7038.
[24] Yang, X., Du, Y., Su, J., Chang, L., Shi, Y. and Lai, J.: 'An Optimal Secondary Voltage Control Strategy for an Islanded Multibus Microgrid. IEEE Journal of Emerging and Selected Topics in Power Electronics, 2016, 4, (4), pp.1236-1246.
[25] Lin, L., Hao Ma, and Bai, Z.: 'An improved proportional load-sharing strategy for meshed parallel inverters system with complex impedances. IEEE Transactions on Power Electronics 32, no. 9 (2017): 7338-7351.
[26] He, J. and Li, Y.W.: 'Analysis, design, and implementation of virtual impedance for power electronics interfaced distributed generation. IEEE Transactions on Industry Applications, 2011, 47, (6), pp.2525-2538.
[27] He, J., Li, Y.W., Guerrero, J.M., Blaabjerg, F. and Vasquez, J.C.: 'An islanding microgrid power sharing approach using enhanced virtual impedance control scheme. IEEE Transactions on Power Electronics, 2013, 28, (11), pp.5272-5282.
[28] Mahmood, H., Michaelson, D. and Jiang, J.: 'Accurate reactive power sharing in an islanded microgrid using adaptive virtual impedances. IEEE Transactions on Power Electronics, 2015, 30, (3), pp.1605-1617.
[29] Zhang, H., Kim, S., Sun, Q. and Zhou, J.: 'Distributed adaptive virtual impedance control for accurate reactive

power sharing based on consensus control in microgrids. IEEE Transactions on Smart Grid, 8, no. 4 (2017), 1749-1761.

[30] Moradi, M.H., Eskandari, M. and Siano, P.: 'Safe transition from connection mode to islanding mode in Microgrids. In Electrical Engineering (ICEE), 2016 24th Iranian Conference on, May 2016, pp. 1902-1907, Shiraz university, Shiraz, Iran.